JOURNAL OF AIRCRAFT
Vol. 45, No. 1, January–February 2008

Decisive Roll of Filling Time on Classification of Parachute Types

F. Mohaghegh* and M. R. Jahannama†
Engineering Research Institute, 13445 Tehran, Iran

DOI: 10.2514/1.29244

In a low altitude recovery, a parachute has to reduce the recovery mass velocity to a predefined velocity before its ground impact within a vertical distance as low as possible. The article classifies various parachutes based on the parachute opening shock and distance necessary to satisfy the steady descent condition in an unreefed situation using numerical solutions of experimental and theoretical relations linked with the parachute opening and flight dynamics. Results show that the parachute filling time is the main parameter to differentiate all parachutes from each other. Based on the parachute filling time, slotted parachutes velocity history coverage locates between ribbon and ringsail parachutes, whereas solid textile parachutes span a range between extended skirt 14.3% and guide surface parachutes. In each group, a decrease in the parachute filling time as a result of the change in the parachute type causes an increase in the parachute opening shock as well as a decrease in the parachute steady distance.

Nomenclature

A	=	parachute area
C_D	=	drag coefficient
C_x	=	opening shock factor
D	=	parachute diameter
F_D	=	parachute drag force
$F_{\max}$	=	opening shock
g	=	gravity acceleration
m	=	total recovery mass
n	=	parachute filling parameter
R_m	=	mass ratio
t	=	elapsed time
t_f	=	parachute filling time
V	=	velocity
X_p	=	parachute shock reduction factor
x	=	parachute filling distance
α	=	correlation coefficient
β	=	power of filling function
γ	=	correlation exponent
ρ	=	air density

Subscripts

O	=	opening instant
p	=	projected
t	=	instant
0	=	nominal

I. Introduction

PARACHUTE deployment and inflation are deemed as two complex aerodynamical processes, and various attempts have been made to elucidate their physical phenomena. These investigations are involved with semiempirical models combining theoretical (i.e., analytical or numerical), and experimental data to gain an insight into the subject. Although recent research takes benefit from high speed computing facilities to obtain more accurate simulations (e.g., [1–4]), the phenomena are still lacking in a physical understanding because of simplifications imposed to the models. This has caused, at least for a short-term scope, more reliance on experimental studies. Nevertheless, owing to the crucial role of the parachute as a dominant recovery tool among the flying systems, this has not dissuaded researchers from the development of theoretical methods that would accelerate the achievement of a better clarification to the phenomena.

The numerical approaches used in the research mainly assume that the deployment and partial inflation have occurred, and thus, it does not cover the consecutive sequences existing throughout the process. In this direction, the studies concern flow analysis within and surrounding the parachute canopy to determine the air velocity and pressure distributions. This is further coupled with the parachute structure to gain a force and in turn a stress analysis on its solid components, which would provide an insight into the canopy displacement and change of shape. This outcome also causes a change in the flow pattern, which necessitates the flow analysis at a new time step. The iteration of this process (i.e., mutual interactions between the flow conditions and the force analysis) implements the parachute simulation (e.g., [1–4]). However, the transient nature of the phenomena and the canopy moving boundaries in conjunction with the coupling of the flow and stress-governing equations raise numerical instability in addition to the need for supercomputers to carry out the time-consuming calculations. Hence, the numerical results mostly rely on two-dimensional and axisymmetric situations, which could not account for a comprehensive simulation.

Parachute experimental studies mainly have focused on either full-scale flight, including payload drop tests (e.g., [5–16]), or subscale wind tunnel investigations (e.g., [16–23]). Behr [8] carried out payload drop tests to study acceleration of a parachute system containing three T-10 reefed parachutes from an altitude as low as 100 m. The results showed that the peak of parachute opening forces occurs before its full opening takes place. Waye [9] developed some experimental flight tests to study opening forces of a 9 m diameter ribbon parachute by which a 344 kg payload from an altitude between 70 to 970 m was recovered. The tests were designed to reduce the payload velocity from 88 to 18 m/s. The results indicated that the maximum acceleration was a linear function of dynamic pressure.

Tyagi and Kumar [18] used a low-speed wind tunnel to analyze the opening of a cross type parachute as infinite mass condition. They also used a sled to conduct a finite mass test. Their results show that the temporal variation of force in the infinite mass condition contains a small decline following the peak, whereas the similar variation in the finite mass condition demonstrates a considerable decline.

Desabrais and Johari [20] investigated temporal variations of canopy-projected diameter, in addition to force and velocity field

Presented as Paper 2527 at the 19th AIAA Aerodynamic Decelerator Systems Technology Conference and Seminar AIAA Balloon Systems Conference, Williamsburg, VA, 21–24 May 2007; received 14 January 2007; revision received 26 August 2007; accepted for publication 1 September 2007.

*Research Assistant, Ministry of Agriculture, Post Office Box 13445-754; fmohaghegh@mail.iust.ac.ir.

†Assistant Professor, Ministry of Agriculture, Post Office Box 13445-754; mjahannama@eri.ac.ir.

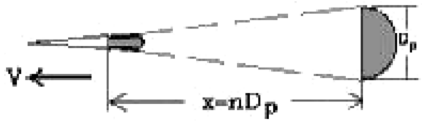

Fig. 1 Filling distance of a parachute canopy.

measurements downstream of the canopy based on a wind tunnel test. The results display the creation of three stages during the parachute opening. In the first stage, there is a linear inflation rate with no wake. The second stage is involved with the formation of wake, causing a maximum drag. In the third stage, the drag force decreases and flow completely separates from the canopy.

It is worth noting that the parachute experimental studies somehow differ from other static experimental research work. The actual parachute tests are mainly concerned with an intrinsic dynamic situation associated with nonrigid canopy developments within a turbulent air flow. Hence, there are twofold complexities involved because of the uncertainty and lack of understanding of flexible material motion further to the random turbulent effects.

Moreover, the uncontrollable surrounding conditions and the unsustainable funding add more limitations to performing a large number of the actual parachute examinations. Thus, theoretical studies are motivated using experimental-based correlations to acquire force history [5–7,10–16,22–32]. In this direction, Berndt and Deweese [5] used parachute opening images to study filling time as well as the variation of canopy projected area. They obtained an experimental relation for parachute filling time proportional to the parachute nominal diameter and in an inverse proportion to the parachute initial velocity.

Potvin et al. [6,7] studied cross type parachutes, both in unreefed and slider-reefed conditions, which were assessed by the data obtained by conducting further flight tests. First, they used a slider reef to delay the parachute inflation [6]. In comparison between theoretical and experimental force histories, parachute opening shock and inflation time showed good agreement. Then they examined an unreefed parachute, whose results approved a higher drag coefficient at the beginning of the inflation (i.e., the minimum drag area) than for the steady-state condition [7].

Potvin [11] established the momentum–impulse theorem to estimate the opening shock factor for maximum parachute force calculation. Integrating parachute motion equation, he calculated the opening shock factor as a function of mass ratio, normalized filling time, and momentum-impulse parameters. The results showed how the higher altitude could produce larger opening forces in a parachute in relation to the mass ratios higher than zero, and that swifter opening leads to larger forces. He extended the method for parachute clusters in [12].

Lee [13,14] obtained a correlation for normalized time and peak opening force in relation with Froude number, stiffness and mass ratio parameters using full and subscale C9 parachutes, which are 8.5 m diameter flat circular personnel parachutes.

Ludtke [15] developed a generic opening shock model that permits calculation of velocity profile and force history during inflation. His calculations indicated that in similar conditions, in the opening of two slotted parachutes with different sizes, the larger parachute had the higher opening shock. However, a solid textile parachute showed an opposite behavior.

Niemi [16] introduced a modified impulse parameter as a product of normalized opening time and opening shock following the study of the parachute opening shock. He also proposed an experimental correlation for the normalized time versus the canopy stiffness index.

Macha [17] proposed an analytical–experimental model that could approximate the changing shape of canopy based on experimental correlations by including radial forces. He conducted a series of wind tunnel tests to verify the theoretical model and concluded that even if the effects of compressibility were neglected, the correlation could be acceptable in velocities below 0.93 Mach number.

Barnard [21] analytically studied the distance necessary to complete parachute inflation using continuity and momentum conservations for fluid flow. He divided the canopy into ring-shaped elements, integrated them over the whole volume of the canopy based on an axisymmetric condition, and obtained a relation for the parachute filling distance. The main result was that the surface density and air density had significant effects on parachute filling time and distance. He concluded that the familiar equation of constant filling distance would be obtained for negligible canopy mass governing the filling process.

Garrard [22] calculated parachute forces during opening stage by a model representing the changes of parachute drag area with time. He also used a 12 m diameter conical parachute carrying a 158 kg payload to produce experimental data for verification of the model. He also showed that there was direct relationship between the Froude number for steady descent and unreefed opening forces.

Doherr [23] developed a method to calculate opening shock factor based on the filling time and drag area experimental relations. He concluded that the opening shock was the sum of three opening shock factors (i.e., analytical expressions of Pflanz [24], Ludtke [25], and a correction term).

Lingard [26] created a model based on relations of added mass, filling time, and parachute temporal projected diameter. He employed the relations in parachute equation of motion with a zero angle of attack and obtained an equation for the parachute deceleration, taking into account forces of gravity, profile drag, deceleration, and growth of added mass.

Johari and Desabrais [27] used dimensional analysis to study the parameters affecting the inflation of solid cloth parachutes. Based on a comparison between sub- and full-scale flat circular C9 parachutes in water and wind tunnels, a relative stiffness index was proposed for filling and opening time correlation.

This article provides a theoretical approach through which the steady state altitude and velocity during a parachute descent would be determined. This is performed using the existing experimental data, implemented with a numerical solution of the differential equation of parachute flight. This equation is derived based on a parachute filling time as a criterion showing the completion of the parachute drag area variation. Solving parachute differential equations for all parachutes, and comparison of results, leads to the parachute sort based on distance necessary to reach the parachute steady descent condition, namely, steady distance. This paper also presents a classification of parachutes based on parachute filling time in unreefed conditions.

Table 1 Characteristic parameters of parachute types [28,30]

Class	No.	Type	C_{Do}	n
Slotted parachutes	1	Flat ribbon	0.45–0.50	14
	2	Conical ribbon	0.50–0.55	14
	3	Ribbon	0.30–0.46	14
	4	Ringslot	0.56–0.65	14
	5	Ringsail	0.75–0.85	7
	6	Disc-gap-band	0.52–0.58	10
Solid textile parachutes	7	Cross	0.60–0.85	11.7
	8	Flat circular	0.75–0.80	8
	9	Conical	0.75–0.90	8
	10	Biconical	0.75–0.92	8
	11	Triconical	0.80–0.96	8
	12	Extended skirt 10%	0.78–0.87	10
	13	Extended skirt 14.3%	0.75–0.90	12
	14	Hemispherical	0.62–0.77	8
	15	Guide surface	0.28–0.42	5
	16	Annular	0.85–0.95	9

II. Modeling

A canopy filling time is defined as the time elapsed during which the stretch of a parachute rope starts until the full inflation of the canopy occurs [28]. In an incompressible flow, a parachute fully opens within a fixed distance, namely, filling distance, regardless of the descent velocity [28]. This stems from the continuity law, which provides a proportional relation between the parachute opening

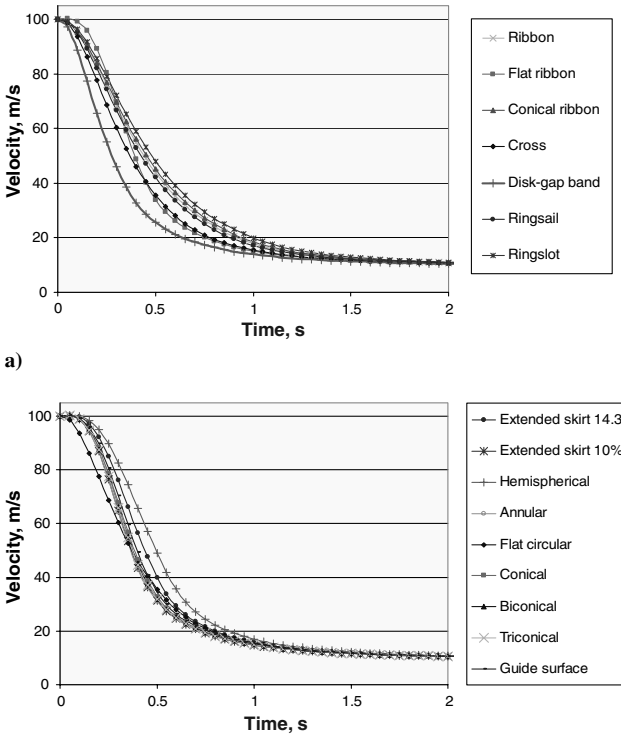

Fig. 2 Variation of velocity vs time for $m = 100$ kg and $V_O = 100$ m/s for parachutes with a) $\beta = 1$; b) $\beta = 2$.

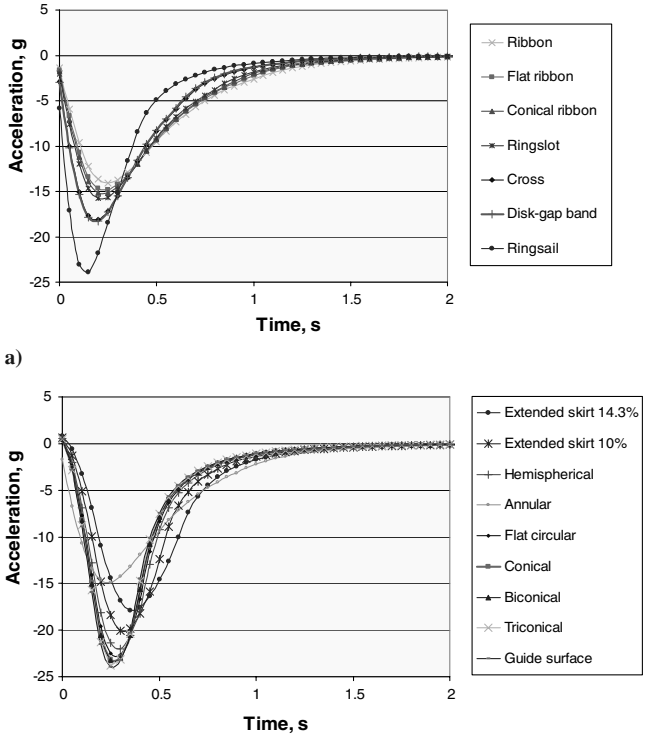

Fig. 3 Variation of acceleration vs time for $m = 100$ kg and $V_O = 100$ m/s for parachutes with a) $\beta = 1$; b) $\beta = 2$.

velocity and its filling flow rate. The parachute filling distance is related to the final projected area given as the following [28]:

$$x = nD_p \tag{1}$$

where x and D_p, as shown in Fig. 1, denote the filling distance and the canopy projected diameter, respectively. Parameter n, known as a parachute filling parameter, is an experimental coefficient depending on the parachute type and porosity as tabulated in Table 1. The values in Table 1 are for the low levels of porosity that grow with an increase in porosity.

Because D_p is a variable parameter given for a certain parachute type and design, depending on rope length, canopy porosity, and parachute material elasticity; a nominal diameter instead is used, which is time independent further to being a standard parameter to compare the diameters of parachutes [28,30]. The nominal diameter is a diameter that is related to the canopy total surface area A_0, including area of the vent and all openings (i.e., $\sqrt{4A_0/\pi}$).

Thus, the parachute filling time based on an assumed constant velocity would be estimated as [6,7,11,23,24,28,30]

$$t_f = \frac{nD_O}{V_O} \tag{2}$$

where t_f and D_O are, respectively, the parachute filling time and nominal diameter and V_O represents the velocity at which the rope starts to stretch. Equation (2) is applicable to all mass ratio ($R_m = \rho(C_D A)^{1.5}/\text{m}$) conditions including drogue parachutes, any parachute inflation in wind tunnels, and general free flight parachutes, except for $R_m > 10$ implying too small descending velocities in which very few parachute applications operate [11].

When the over inflation is ignored, variation of drag area during the air filling process could be determined [28]. Solid textile parachutes, which have a continuous geometrical shape without slots, usually are used as a main descent parachute. In these parachutes, except for cruciform or cross type parachutes, the rate of

Table 2 Parachute sort based on steady distance for $m = 100$ kg and $V_O = 100$ m/s

		Parachute type	Steady distance, m	Filling time, s	Maximum acceleration, g	t_O	t_O/t_f
$\beta = 1$	1	Ribbon	79.76	1.039	14.12	0.270	0.261
	2	Flat ribbon	76.72	0.929	14.94	0.250	0.269
	3	Conical ribbon	75.42	0.884	15.32	0.250	0.283
	4	Ringslot	73.53	0.824	15.90	0.239	0.290
	5	Cross	67.41	0.629	18.23	0.211	0.332
	6	Disk gap band	67.11	0.616	18.41	0.210	0.326
	7	Ringsail	58.23	0.358	24.24	0.159	0.421
$\beta = 2$	1	Extended skirt 14.3%	78.67	0.604	17.94	0.379	0.627
	2	Extended skirt 10%	73.3	0.503	20.26	0.342	0.679
	3	Hemispherical	69.65	0.438	22.19	0.313	0.714
	4	Annular	69.33	0.433	22.36	0.309	0.714
	5	Flat circular	68.42	0.415	23.48	0.300	0.722
	6	Conical	67.77	0.403	23.34	0.295	0.733
	7	Biconical	67.58	0.400	23.57	0.295	0.734
	8	Triconical	66.95	0.390	23.94	0.288	0.738
	9	Guide surface	66.84	0.386	24.14	0.286	0.741

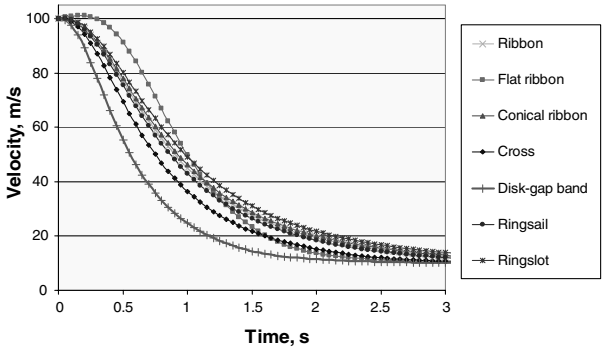

a)

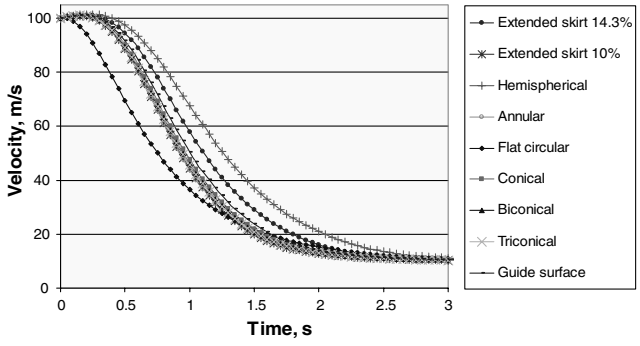

b)

Fig. 4 Variation of velocity vs time for $m = 1500$ kg and $V_O = 100$ m/s for parachutes with a) $\beta = 1$; b) $\beta = 2$.

canopy inflation or drag area rises with time. Here it is assumed that the drag area variation is a second order function of time without reefing [22,23,28]. Slotted parachutes contain slots and gaps in the canopy, which cause powerful stability and low opening forces. In the slotted and cross parachutes in unreefed conditions, the variation of temporal drag area is a linear function of time [22,23,28]. Therefore, for all parachutes, the instant drag area [i.e., $(C_DA)_t$] during the parachute inflation in unreefed conditions could be written as the following:

$$(C_DA)_t = (C_DA)_0\left(\frac{t}{t_f}\right)^{\beta} \tag{3}$$

where $(C_DA)_0$ is the nominal drag area or the drag area in steady descent condition. Power β is equal to one for slotted and cross parachutes and is equal to two for other types of parachutes [22,23,28]. (For reefed parachutes, these references recommend 0.5 for β. See [15,23,25], which also recommend $\beta = 6$ for solid cloth parachutes).

Because air flow regime during whole parachute descent time is turbulent, the drag force is proportional to the squared velocity as given by [31]:

$$F_D = \tfrac{1}{2}\rho(C_DA)_tV^2 \tag{4}$$

where V is the instant velocity of the recovery system. Thus, Newton's second law for a vertical descent of the recovery system may be rearranged as

$$m\frac{\mathrm{d}V}{\mathrm{d}t} = mg - \frac{1}{2}\rho(C_DA)_tV^2 \tag{5}$$

Equation (5) is known as the parachute differential equation. Substitution of Eq. (3) in Eq. (5) leads to

$$m\frac{\mathrm{d}V}{\mathrm{d}t} = mg - \frac{1}{2}\rho(C_DA)_0V^2\left(\frac{t}{t_f}\right)^{\beta} \tag{6}$$

To solve the previous equation, the following initial condition is needed:

$$V = V_O \quad \text{at } t = 0 \tag{7}$$

A solution for Eq. (6) should be sought in two stages. The first stage is linked with the parachute filling process (i.e., $0 < t < t_f$), during which the drag area increases. In this period, the development of drag area depends on the parachute type, which necessitates the parameter β [Eq. (3)] to be either one or two. The second stage is related to the parachute descent following its full inflation (i.e., $t > t_f$). Because this stage occurs when the drag area is completely developed, the role of the parameter β should be omitted. In other words, Eq. (6) was derived provided that the parachute was under inflation. After the parachute's full inflation is acquired, the drag area will remain constant and independent of the parachute type. In this situation, the parameter β would be set to zero.

The parachute differential equation [i.e., Eq. (6)], is a nonlinear equation whose analytical solution does not seem to be straightforward. Moreover, this equation is not a regular Riccati differential equation, as the extra factor t^{β} exists. It is clear that the analytical solutions to the parachute differential equation appear to be complex to use (they also have to be integrated to obtain the distance). On the other hand, the numerical solutions are easy and could be applied with an explicit solution. To attain the solution, a computer code based on Visual Basic has been programmed. This code has run to obtain numerical results using a time step less than

Table 3 Parachute sort based on steady distance for $m = 1500$ kg and $V_O = 100$ m/s

		Parachute type	Steady distance, m	Filling Time, s	Maximum acceleration, g	t_O	t_O/t_f
$\beta = 1$	1	Ribbon	152.38	4.023	7.050	0.552	0.137
	2	Flat ribbon	142.65	3.598	7.468	0.522	0.145
	3	Conical ribbon	138.60	3.422	7.664	0.508	0.148
	4	Ringslot	133.13	3.186	7.951	0.489	0.153
	5	Cross	115.44	2.433	9.135	0.425	0.175
	6	Disk gap band	114.33	2.387	9.224	0.421	0.176
	7	Ringsail	89.30	1.386	12.188	0.316	0.228
$\beta = 2$	1	Extended skirt 14.3%	159.41	2.340	7.397	0.965	0.412
	2	Extended skirt 10%	142.45	1.950	8.326	0.855	0.438
	3	Hemispherical	131.31	1.699	9.107	0.779	0.458
	4	Annular	130.43	1.679	9.175	0.769	0.458
	5	Flat circular	127.21	1.608	9.439	0.749	0.466
	6	Conical	124.99	1.560	9.629	0.734	0.470
	7	Biconical	124.57	1.550	9.668	0.730	0.471
	8	Triconical	122.74	1.510	9.836	0.718	0.475
	9	Guide surface	122.09	1.496	9.895	0.713	0.477

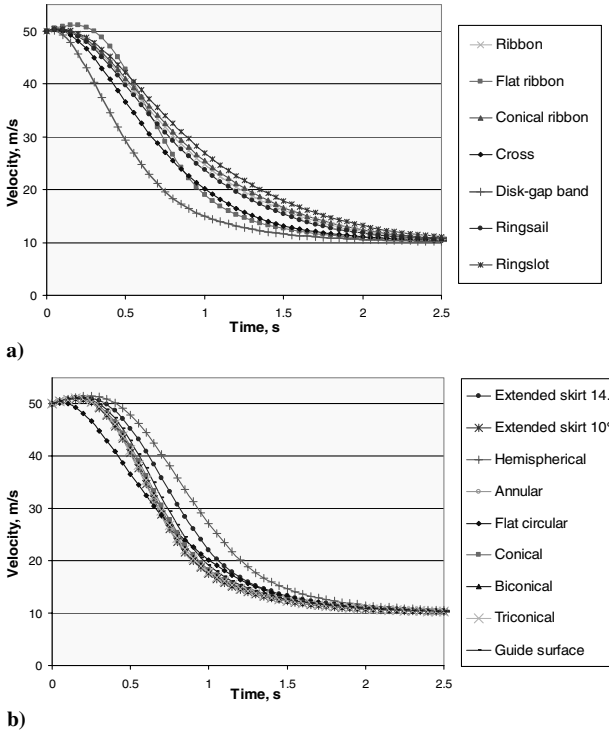

Fig. 5 Variation of velocity vs time for $m = 100$ kg and $V_O = 50$ m/s for parachutes with a) $\beta = 1$; b) $\beta = 2$.

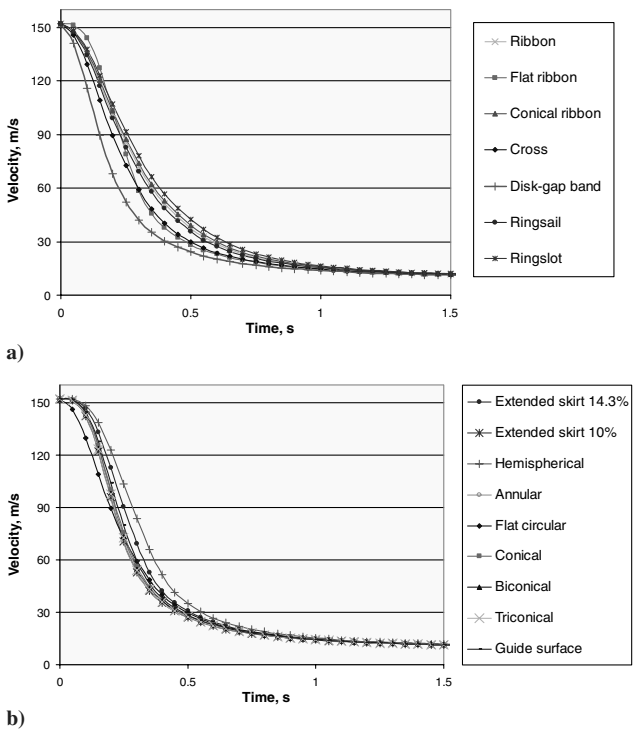

Fig. 6 Variation of velocity vs time for $m = 100$ kg and $V_O = 152$ m/s for parachutes with a) $\beta = 1$; b) $\beta = 2$.

0.0001 s with a convergence criterion of reaching a factor of 1.01 for the steady descent velocity (saying that the steady factor is 1.01 or SF = 1.01). To test the independency of results from the time step, three time steps were implemented: 0.01, 0.001, and 0.0001 s. The results coincided well with each other, confirming their independency from the time step.

III. Results

Results are obtained for all parachute types, provided that the parachute final velocity approaches 10 m/s, resulting in a steady descent motion. As the altitude of recovery is very low, say 200 m, the variation of air density is neglected. The results are presented for the various parachutes, which carry a recovery system of known mass and initial velocity and a steady-state factor (SF) of 1.01.

Time history of velocity is shown in Fig. 2 for both parachute groups [i.e., slotted and cross ($\beta = 1$) and solid textile ($\beta = 2$)]. These results are given based on a recovery system of 100 kg with an initial velocity equal to 100 m/s. Figure 2 shows a decreasing trend for the velocity distribution, leading to a constant velocity that demonstrates the steady descent condition. The sharp decrease in velocity explains the parachute inflation process, which is engaged with an increase in the canopy area causing a rise in drag force. Following the inflation, a parachute needs more time to reach a steady descent condition, which causes the continuation of the sharp decrease before the constant steady velocity. Thus, the time needed for the decreasing trend of the velocity distribution is created because of the inflation as well as the steady state duration after the inflation. Figure 2 also shows the dependency of the decreasing rate of velocity on the parachute type, which implies the role of a parachute structure on the aerodynamics of the inflating air flow. The parachute structure affects the filling parameter and drag coefficient (as seen in Table 1), which causes, for instance, the velocity trend to lie between the ringsail and ribbon parachutes as shown in Fig. 2a.

Figure 3 shows the variation of acceleration versus time for two classes of parachutes. In all cases and throughout the descent, there is a negative acceleration implying a decrease in velocity until the descent becomes steady. The figure indicates that there is an extreme acceleration for each parachute. This acceleration explains the

Table 4 Parachute sort based on steady distance for $m = 100$ kg and $V_O = 50$ m/s

		Parachute type	Steady distance, m	Filling time, s	Maximum acceleration, g	t_O	t_O/t_f
$\beta = 1$	1	Ribbon	78.03	2.078	3.363	0.590	0.284
	2	Flat ribbon	74.11	1.858	3.566	0.559	0.301
	3	Conical ribbon	72.47	1.767	3.661	0.542	0.307
	4	Ringslot	70.14	1.645	3.802	0.521	0.317
	5	Cross	62.74	1.257	4.380	0.449	0.357
	6	Disk gap band	62.36	1.233	4.423	0.447	0.363
	7	Ringsail	52.14	0.716	5.573	0.336	0.469
$\beta = 2$	1	Extended skirt 14.3%	74.71	1.207	4.648	0.793	0.657
	2	Extended skirt 10%	68.57	1.007	5.218	0.701	0.696
	3	Hemispherical	64.48	0.877	5.700	0.639	0.728
	4	Annular	64.13	0.867	5.740	0.633	0.730
	5	Flat circular	63.10	0.830	5.901	0.616	0.742
	6	Conical	62.36	0.805	6.018	0.601	0.746
	7	Biconical	62.16	0.801	6.042	0.601	0.750
	8	Triconical	61.46	0.780	6.144	0.590	0.756
	9	Guide surface	61.33	0.773	6.182	0.585	0.757

Table 5 Parachute sort based on steady distance for $m = 100$ kg and $V_O = 152$ m/s

		Parachute type	Steady distance, m	Filling time, s	Maximum acceleration, g	t_O	t_O/t_f
$\beta = 1$	1	Ribbon	83.02	0.683	32.99	0.177	0.259
	2	Flat ribbon	80.14	0.611	34.90	0.168	0.275
	3	Conical ribbon	78.91	0.581	35.79	0.163	0.280
	4	Ringslot	77.11	0.541	37.10	0.158	0.292
	5	Cross	71.22	0.413	42.50	0.137	0.332
	6	Disk gap band	70.94	0.406	42.91	0.136	0.335
	7	Ringsail	62.31	0.235	56.43	0.103	0.438
$\beta = 2$	1	Extended skirt 14.3%	82.34	0.397	41.29	0.252	0.635
	2	Extended skirt 10%	77.12	0.331	46.61	0.223	0.673
	3	Hemispherical	73.56	0.289	51.07	0.204	0.706
	4	Annular	73.24	0.285	51.47	0.202	0.709
	5	Flat circular	72.36	0.273	52.97	0.196	0.718
	6	Conical	71.72	0.265	54.06	0.192	0.725
	7	Biconical	71.54	0.263	54.28	0.191	0.726
	8	Triconical	70.92	0.257	55.23	0.188	0.732
	9	Guide surface	70.81	0.254	55.58	0.186	0.732

parachute opening shock, which causes a sudden change in the parachute acceleration leading to its full inflation. The force acting on the parachute comprises two parts (i.e., drag area and velocity squared). Before the shock point, the effect of an increase in drag area on the acting force dominates the effect of a decrease in the velocity squared. On the contrary, after the shock point, these two parts exchange their roles with each other.

Table 2 shows the parachutes based on their steady distance corresponding to Figs. 2 and 3. With reference to Table 1, it is clear that a greater filling parameter leads to a larger steady distance as shown in Table 2.

From Eq. (6), for each group of parachutes with specified recovery mass, initial velocity, and drag area, this is t_f, which can be changed and thus be considered as a criterion for the variation of velocity and, in turn, the altitude.

Table 2 also shows an increase in the maximum acceleration with a decrease in the filling time. This also causes a reduction of the period needed for the occurrence of the opening shock or t_O. Referring to Table 2, despite the similar trends of the filling time and the opening shock instant, the ratio of these two parameters reflected on t_O/t_f shows that the filling time has a greater rate of decrease compared with the opening shock instant.

One of the main differences between the two groups of parachutes is distinguished in Table 2 based on the t_O/t_f parameter. This parameter shows higher values for the solid textile parachutes ($\beta = 2$) compared with the slotted parachutes ($\beta = 1$). The reason is that for the parachutes with $\beta = 1$, the development of drag area and, in consequence, its corresponding force initially has a higher rate than for the parachutes with $\beta = 2$. This shifts the opening shock to an earlier instant for the slotted parachutes than for the solid textile parachutes.

In addition, Table 2 shows that the parachutes with greater filling times have smaller parachute opening shocks. Because a decrease in the filling time shortens the period needed for a maximum drag area, the rate of decrease in velocity (acceleration or index of force) is strengthened, raising the opening shock force.

Figure 4 shows similar trends for the time history of velocity at a different recovery mass (i.e., 1500 kg) for the same steady descent velocity (i.e., 10 m/s) compared with Fig. 2. The main difference between Fig. 2 and Fig. 4 lies in an increase in velocity during the first instants of inflation as the recovery mass increases; this is more evident in Fig. 4b. An increase in the recovery mass at a constant initial velocity causes a higher gravity force, which dominates the drag force at the commencement of inflation leading to an increase in velocity. However, this lasts only for a very short time, and thereafter, the deceleration begins because of the air filling, which causes the domination of the drag force. This, seen in Fig. 4, however, prolongs the unsteady descent condition compared with Fig. 2.

Table 3 lists the corresponding data of Fig. 4. A comparison between Tables 2 and 3 indicates that as the recovery mass increases, the filling time would be estimated as $\sqrt{1500/100} \cong 3.87$. This is based on the following:

$$\left.\begin{aligned} t_f &= \tfrac{nD_O}{V_O} \\ mg &= \tfrac{1}{2}\rho C_{D_O} A_0 V_{\text{steady}}^2 \Rightarrow D_O = \sqrt{\tfrac{8mg}{\pi\rho C_D V_{\text{steady}}^2}} \end{aligned}\right\} \Rightarrow \frac{t_{f_2}}{t_{f_1}} = \sqrt{\frac{m_2}{m_1}} \quad (8)$$

The increase in the filling time also implies a greater distance required to reach the steady descent condition as can be seen by comparing Tables 2 and 3. Table 2, when compared with Table 3, also shows that the increase in the parachute recovery mass imposes a smaller maximum acceleration (i.e., a smaller opening shock). This is because the mass increase entails a larger drag area to reach the same final velocity. Thus, a larger drag area and, in turn, a greater filling time, prolong the air filling process, which reduces the opening shock influence reflecting a smaller maximum acceleration. Table 3 also shows higher values of t_O/t_f for the solid textile parachutes ($\beta = 2$)

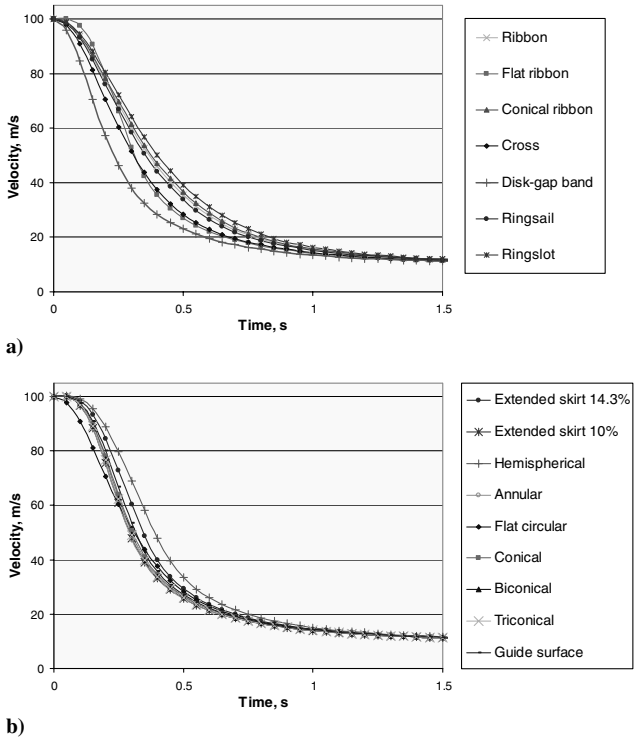

Fig. 7 Variation of velocity vs time for $m = 50$ kg and $V_O = 100$ m/s for parachutes with a) $\beta = 1$; b) $\beta = 2$.

Table 6 Parachute sort based on steady distance for $m = 50$ kg and $V_O = 100$ m/s

		Parachute type	Steady distance, m	Filling time, s	Maximum acceleration, g	t_O	t_O/t_f
$\beta = 1$	1	Ribbon	68.74	0.735	16.84	0.229	0.312
	2	Flat ribbon	66.27	0.657	17.82	0.216	0.329
	3	Conical ribbon	65.38	0.625	18.28	0.211	0.338
	4	Ringslot	63.94	0.582	18.96	0.203	0.349
	5	Cross	59.42	0.444	21.73	0.177	0.399
	6	Disk gap band	59.01	0.436	21.95	0.175	0.401
	7	Ringsail	52.24	0.253	28.90	0.133	0.526
$\beta = 2$	1	Extended skirt 14.3%	66.83	0.427	22.59	0.305	0.714
	2	Extended skirt 10%	62.85	0.356	25.49	0.271	0.761
	3	Hemispherical	60.53	0.310	27.92	0.246	0.794
	4	Annular	60.13	0.307	28.14	0. 245	0.798
	5	Flat circular	59.45	0.294	28.96	0.238	0.806
	6	Conical	58.77	0.285	29.55	0.234	0.821
	7	Biconical	58.63	0.283	29.67	0.233	0.823
	8	Triconical	58.59	0.276	30.19	0.228	0.826
	9	Guide surface	58.29	0.273	30.38	0.226	0.828

Table 7 Parachute correlation parameters for Eq. (10)

Class	No.	Type	α	R_m threshold
$\beta = 1$	1	Flat ribbon	0.54	0.4
	2	Conical ribbon	0.52	0.3
	3	Ribbon	0.63	0.3
	4	Ringslot	0.48	0.3
	5	Ringsail	0.56	0.25
	6	Disk gap band	0.59	0.3
	7	Cross	0.50	0.25
$\beta = 2$	1	Flat circular	0.85	0.5
	2	Conical	0.85	0.5
	3	Biconical	0.84	0.5
	4	Triconical	0.83	0.5
	5	Extended skirt 10%	0.75	0.3
	6	Extended skirt 14.3%	0.75	0.3
	7	Hemispherical	0.88	0.5
	8	Guide surface	1.31	1.8
	9	Annular	0.80	0.4

compared with the slotted parachutes ($\beta = 1$), which confirms the similar findings as cited in Table 2. In overall, Tables 2 and 3 show similar trends for different parameters listed, which confirms the null influence of the recovery mass and, in turn, the drag area on the parachute categorization.

Figure 5 shows the time history of velocity for the same conditions of Fig. 2 but at a smaller initial velocity (i.e., 50 m/s). A decrease in initial velocity for a certain recovery mass leads to a decrease in drag force. Therefore, the accelerating motion within the initial instants should become more apparent, as can be seen in Fig. 5. This is in good agreement with the corresponding description given on Fig. 2. In addition, a comparison between Fig. 2 and Fig. 5 shows that the smaller initial velocity postpones the attainment of descent condition because of the higher required filling time. This, as seen in Fig. 5, also affects the separation of the velocity curves assigned to each parachute, which highlights the parachute structure role.

Table 4 lists the corresponding data of Fig. 5, illustrating the similar trends as seen in Table 2. It can be seen that the lower initial velocity leads to a smaller maximum acceleration as compared with Table 2. Moreover, a comparison between Tables 2 and 4 shows that to theoretically halve the initial velocity (from 100 to 50 m/s) results in an approximately quarter reduction of the opening shock. This may be compared to a correlation used to calculate the opening shock as given by [6,7,10,12,23–29]

$$F_{\max} = \tfrac{1}{2}\rho C_x X_p (C_D A)_0 V_O^2 \tag{9}$$

where C_x and X_p denote parachute opening shock factor and parachute shock reduction factor, respectively. From Eq. (9), it is evident that the opening shock (as an index of acceleration) is proportional to the square of initial velocity. Thus, the same result as mentioned previously can be deduced. In other words, because the mass ratio $R_m = \rho(C_D A)^{1.5}/m$ has the same order of magnitude for both parachutes, the shock reduction factor acquires approximately the same value for both cases [11,12].

To provide a further insight into the aforementioned investigations regarding the roles of mass and initial velocity, supplementary simulations have been carried out to cover a broader range of these two parameters. In this direction, two more simulations are performed with the same steady descent velocity (i.e., 10 m/s). The first simulation is performed with an initial velocity of 152 m/s. Based on Knacke [28], Eq. (2) is valid in a range between 46 to 152 m/s, regardless of compressibility. Because the lower limit was

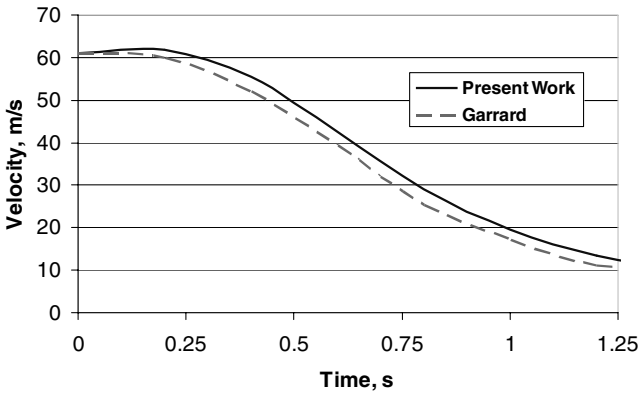

Fig. 8 Comparison of results with Garrard's theoretical work.

investigated in Fig. 5 and Table 4 for 50 m/s, the upper limit (152 m/s) needs simulation. The simulation results are plotted in Fig. 6 and listed in Table 5. They show similar trends to Fig. 2 and the same arrangement of parachute types as listed in Table 4. With reference to Tables 2, 4, and 5, it can be seen that t_O/t_f attains similar order of magnitude for each type of parachute with similar recovery masses, which would confirm the uniqueness of t_O/t_f through the whole range of initial velocity (50 to 152 m/s) for similar recovery masses. Moreover, regarding the ratio of initial velocities (i.e., 152/100 and 152/50), the maximum acceleration in Table 5 finds a growth factor of $(1.52)^2$ and $(3.04)^2$ of the maximum acceleration listed in Tables 2 and 4, respectively. This agrees with Eq. (9), wherein the opening shock is proportional to the square of initial velocity.

The next simulation considers a recovery mass of 50 kg, while the initial velocity has been fixed to 100 m/s. The results are presented in Fig. 7 and Table 6. The results display similar trends and parachute arrangements as achieved in Figs. 2 and 4 as well as Tables 2 and 3. However, a comparison between Tables 3 and 6 shows that an increase in the recovery mass from 50 to 1500 kg leads to decreases in t_O/t_f and opening shock factor. This agrees with [20,22,28], in which the variation of opening shock factor with respect to mass ratio $R_m = \rho(C_D A)^{1.5}/m$ confirms that an increase in the mass ratio reduces the parachute opening shock.

Comparison of Tables 2, 3, and 5 shows a same trend for the effect of recovery mass on filling time and maximum acceleration. Based on Eq. (8), the filling time in Table 6 equals $\sqrt{50/100} \cong 0.7$ of that in Table 2.

According to [12], t_O/t_f as a function of R_m approaches unity when R_m reduces to zero. Based on this, a correlation would be developed for the results obtained in this work as the following:

$$t_O/t_f = \alpha(R_m)^{\gamma} \tag{10}$$

where the exponent γ is $\frac{1}{2}$ for parachutes with $\beta = 1$ and $\frac{1}{3}$ for parachutes with $\beta = 2$, respectively. Equation (10) could be used for all parachutes investigated in this work provided that the parameters α and R_m obey the values tabulated in Table 7. This should be noted that R_m contains a threshold for each type of parachute below which t_O/t_f is approximately unity. This agrees with [12,23,27].

IV. Validation of Results

To evaluate the results, the work of Garrard [22] has been selected. Garrard reported on an 11.5 m diameter conical parachute used to recover a 158 kgf mass from a velocity of 61 to 6.5 m/s. Figure 8 shows a good agreement between the present work and the work of Garrard. However, the present work shows a little greater velocity, as Garrard, in his work, discarded the gravity effects.

As a further comparison, the results are compared with the data of Strickland and Macha [32] who used a 3 m construction diameter ringslot parachute with a porosity of 20%. The parachute had to recover a 13.6 kgf mass from 76.4 m/s velocity to 8.5 m/s in a vertical motion. The comparison is presented in Fig. 9, which shows a good agreement between the present work and the experimental data. However, there is a little deviation from the experimental data at the first stages of opening. This is because of the inclusion of vehicle and pilot chute drag in the work of Strickland and Macha, whereas in the present work the initial drag area is zero, and only the main parachute affects the drag of system. In addition, it should be mentioned that there is not any wake recontact in the present research, whereas the wake recontact exists in the work of Strickland and Macha.

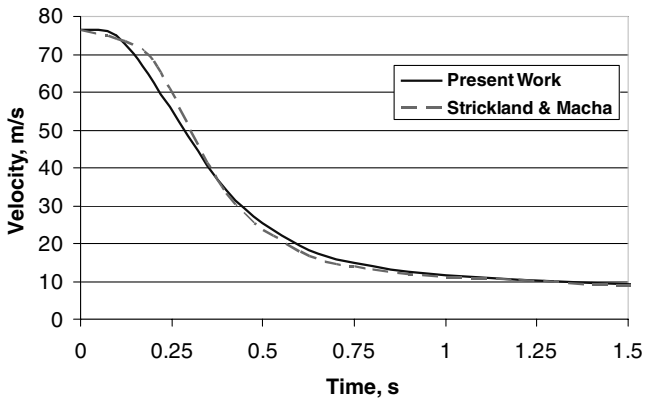

Fig. 9 Comparison of results with Strickland and Macha's experimental work.

V. Conclusions

The parachute flight dynamics equation, using the parachute drag area changes with time during inflation and constant canopy shape after inflation, is a proper approximation for the parachute simulation during and after the inflation.

The results show the dependency of decreasing rate of velocity on the parachute type, which implies the role of a parachute structure on aerodynamics of the inflating air flow. The parachute structure affects the filling time and drag coefficient which cause the velocity trend to, respectively, lie between the ringsail and ribbon parachutes for slotted parachutes and between extended skirt 14.3% and guide surface parachutes for solid textile parachutes.

Throughout the descent in all cases (except for very initial instants of opening, in some cases, with low initial velocity), there is a negative acceleration implying a decrease in velocity until reaching steady descent condition. There is an extreme acceleration for each parachute. This acceleration explains the parachute opening shock, after which the parachute acceleration reduces because of a sharp decrease in the parachute velocity.

The results illustrate that the parachute filling time is the main parameter that determines the distance necessary to reach the steady state condition further to the parachute opening shock. It has been proved that the greater filling parameter leads to a larger steady distance. Another confirmation was the existence of an increase in the maximum acceleration with a decrease in the filling time. This decrease also causes a reduction of the period needed for the occurrence of the opening shock. Although the filling time and the opening shock instant have similar trends, the ratio of these two parameters shows that the filling time has a greater rate of decrease compared with the opening shock instant. The ratio of the opening shock instant to the filling time shows higher values for the solid textile parachutes than for the slotted parachutes. This is because of the fact that the development of drag area, and, in consequence, its corresponding force for slotted parachutes, has a higher rate of growth than for the solid textile parachutes. This shifts the opening shock to an earlier instant for the slotted parachutes.

It has been indicated that the parachutes with greater filling times have smaller parachute opening shock. Because a decrease in the filling time shortens the period needed for a maximum drag area, the rate of decrease in velocity (acceleration or an index of force) is strengthened, rising the opening shock force.

The simulations on a broader range of initial velocity and recovery mass illustrate similar trends of velocity variation as well as the parachute arrangement in terms of filling time, maximum acceleration, and t_O/t_f, which further confirms the consistency of the method used to investigate the subject. Whenever either recovery mass or initial velocity has been decreased, there will be an increase in velocity during the first instant of inflation. With increase of recovery mass or decrease of initial velocity, there will be an increase in velocity during the first instant of inflation, leading to an increase in the parachute velocity. The smaller initial velocity postpones the attainment of steady descent condition because of the higher filling time required

The ratio of the opening shock instant to filling time would be correlated in terms of the parachute recovery mass. This correlation is given using two tuning parameters that cover the whole range of the parachutes investigated in this study. In addition, this correlation is associated with a threshold of the recovery mass ratio for each parachute below which the ratio remains at approximate unity.

References

[1] Kim Y., and Peskin, C. S., "2-D Parachute Simulation by the Immersed Boundary Method," *SIAM Journal on Scientific Computing*, Vol. 28, No. 6, 2006, pp. 2294–2312. doi:10.1137/S1064827501389060

[2] Benney, R. J., and Stein, K. R., "A Computational Fluid-Structure Interaction Model for Parachute Inflation," *Journal of Aircraft*, Vol. 33, No. 4, 1996, pp. 730–736.

[3] Johari, H., and Desabrais, K. J., "A Coupled Fluid-Structure Parachute Inflation Model," AIAA Paper 2003-2146, 19–22 May 2003.

[4] Tutt, B. A., and Taylor, A. P., "The Use of LS-DYNA to Simulate the Inflation of a Parachute Canopy," AIAA Paper 2005-1608, 23–26 May 2005.

[5] Berndt, R. J., and Deweese, J. H., "A Filling Time Prediction Approach for Solid Cloth Type Parachute Canopies," *2nd AIAA Aerodynamic Decelerator Systems Technology Conference*, AIAA, New York, 7–9 Sept. 1966, pp. 17–32.

[6] Potvin, J., Peek, G., Brocato, B., Perschbacher, T., and Kutz, R., "Inflation and Glide Studies of Slider Reefed Cruciform Parachutes," *AIAA 16th Aerodynamic Decelerator Systems Technology Conference*, AIAA, Reston, VA, 21–214 May 2001, pp. 194–212.

[7] Potvin, J., Peek, G., Brocato, B., Manglano, C., and Kutz, R., "Deceleration Dynamics of Unreefed Cruciform and Flat Circular Parachutes During and After Inflation," *AIAA 16th Aerodynamic Decelerator Systems Technology Conference*, AIAA, Reston, VA, 21_24 May 2001, pp. 224–234.

[8] Behr, V. L., "The Design and Flight Testing of a High Performance, Low Cost Parachute System for a 1000 lb Payload," *AIAA 11th Aerodynamic Decelerator System Technology Conference*, AIAA, Washington, D.C., 9–11 April 1991, pp. 366–373.

[9] Waye, D. E., "Design and Performance of Parachute for Recovery of 760 lb Payload," *AIAA 11th Aerodynamic Decelerator System Technology Conference*, AIAA, Washington, D.C., 9–11 April 1991, pp. 374–383.

[10] Wolf, D., "Parachute Opening Shock," *15th CEAS/AIAA Aerodynamic Decelerator Systems Technology Conference*, AIAA, Reston, VA, 8–11 June 1999, pp. 253–257; also AIAA Paper 99-1702.

[11] Potvin, J., "Universality Considerations for Graphing Parachute Opening Shock Factor Versus Mass Ratio," *Journal of Aircraft*, Vol. 44, No. 2, March–April 2007, pp. 528–538. doi:10.2514/1.24061

[12] Potvin, J., "Momentum-Impulse Balance and Parachute Inflation: Clusters," *Journal of Aircraft*, Vol. 44, No. 2, March–April 2007, pp. 687–691. doi:10.2514/1.26285

[13] Lee, C. K., "Experimental Investigation of Full-Scale and Model Parachute Opening," *8th AIAA Aerodynamic Decelerator and Balloon Technology Conference*, AIAA, New York, 2–4 April 1984, pp. 215–223; also AIAA Paper 84-0820.

[14] Lee, C. K., "Modeling of Parachute Opening: an Experimental Investigation," *Journal of Aircraft*, Vol. 26, No. 5, May 1989, pp. 444–451.

[15] Ludtke, W. P., "Notes on a Generic Parachute Opening Force Analysis," *AIAA 9th Aerodynamic Decelerator and Balloon Technology Conference*, AIAA, New York, 7–9 Oct. 1986, pp. 72–85.

[16] Niemi, E. E., Jr., "An Impulse Approach for Determining Parachute Opening Loads for Canopies of Varying Stiffness," *11th AIAA Aerodynamic Decelerator Systems Technology Conference*, AIAA, Washington, D.C., 9–11 April 1991, pp. 313–321; also AIAA Paper 91-0874.

[17] Macha, J. M., "A Simple, Approximate Model for Parachute Inflation," *AIAA 12th Aerodynamic Decelerator System Technology Conference*, AIAA, Washington, D.C., 10–13 May 1993, pp. 44–53.

[18] Tyagi, J. K., and Kumar, P., "Parametric Study of Unicross Parachute under Infinite and Finite Mass Conditions," *AIAA 11th Aerodynamic Decelerator System Technology Conference*, AIAA, Washington, D.C., 9–11 April 1991, pp. 304–309; also AIAA Paper 91-0872.

[19] Render, A. B., and Bradley, P. D., "The Development of a Parachute Strain Measurement Technique," *AIAA 9th Aerodynamic Decelerator and Balloon Technology Conference*, AIAA, New York, 7–9 Oct. 1986, pp. 194–202.

[20] Desabrais, K. J., and Johari, H., "The Flow in the Near Wake of an Inflating Parachute Canopy," *AIAA 16th Aerodynamic Decelerator Systems Technology Conference*, AIAA, Reston, VA, 21–24 May 2001, pp. 122–130; also AIAA Paper 2001-2009.

[21] Barnard, G. A., "The Effect of Extreme Altitude on Parachute Filling Distance," *AIAA 12th Aerodynamic Decelerator System Technology Conference*, AIAA, Washington, D.C., 10–13 May 1993, pp. 54–61.

[22] Garrard, W. L., "Application of Inflation Theories to Preliminary Parachute Force and Stress Analysis," *AIAA 11th Aerodynamic Decelerator System Technology Conference*, AIAA Paper 91-0862, Washington, D.C., 9–11 April 1991, pp. 230–239.

[23] Doherr, K. F., "Extended Parachute Opening Shock Estimation Method," AIAA Paper 2003-2173, 9–22 May 2003.

[24] Pflanz, E., "Zur Bestimmung der Verzoegerunskraefte bei Entfaltung von Lastenfallschirmen," Forschungsannstalt Graf Zeppelin, Stuttgart-Ruit, Bericht, 1942 (Published as ZWB FB 1706 in 1942).

[25] Ludtke, W. P., "A Technique for the Calculation for the Opening-Shock Forces for Several Types of Solid Cloth Parachutes," *4th AIAA Aerodynamic Decelerator Systems Technology Conference*, AIAA, New York, 21–23 May 1973, pp. 176–185; also AIAA Paper 73-477.

[26] Lingard, J. S., "The Effects of Added Mass on Parachute Inflation Force Coefficients," *13th AIAA Aerodynamic Decelerator Systems Technology Conference*, AIAA, Washington, D.C., 15–18 May 1995, pp. 176–185; also AIAA Paper 95-1561.

[27] Johari, H., and Desabrais, K. J., "Stiffness Scaling for Solid-Cloth Parachutes," *Journal of Aircraft*, Vol. 40, No. 4, July–Aug. 2003, pp. 631–637.

[28] Knacke, T. W., "Parachute Recovery Systems Design Manual," *Parachute Recovery and Performances*, 1st ed., Para Publishing Co., Santa Barbara, CA, 1992, pp. 3–5, 41–56, Chap. 5.

[29] French, K. E., "The Initial Phase of Parachute Inflation," *3rd AIAA Aerodynamic Decelerator Systems Technology Conference*, AIAA, New York, 23–25 Sept. 1968.

[30] Poynter, D., "The Parachute Manual," *Parachute Design and Construction*, 3rd ed., Para Publishing Co., Santa Barbara, CA, 1984, pp. 457–470.

[31] White, F. M., "Fluid Mechanics," *Flow Past Immersed Boddies*, 4th ed., McGraw–Hill, New York, 2001, pp. 438–469.

[32] Strickland, J. H., and Macha, J. M., "A Preliminary Characterization of Parachute Wake Recontact," *10th AIAA Aerodynamic Decelerator Systems Technology Conference*, AIAA, Washington, D.C., 18–20 April 1989, pp. 78–85; also AIAA Paper 89-0897.